Parametric Performance Analysis of a Vertical Axis Wind Turbine

Yang Cao, Jinyi Li, Guoqing Wu, Qiaomei Li, Yujuan Shi, Shuda Xing

ABSTRACT

As the power efficiency is affected by every aspect of a wind turbine and its blades, a 2D-computational investigation of several key parameters is proposed after which actual experiments are performed. Six parameters are examined in the computational investigation: installation angle; blade airfoil; chord length; number of blades; radius of an impellor; and wind speed. To find out the optimum performance of a Vertical Axis Wind Turbine or VAWT, one appropriate parameter is selected at each section of the simulation progression. Afterwards, an experimental prototype of wind turbine is fabricated and put into an airdynamic test to ascertain the validity of the previous CFD simulation.

Keywords: CFD simulation, Darrieus type, parameter, solidity, spin-up method, VAWT

INTRODUCTION

The Darrieus type wind turbine was first invented by a French engineer G.J.M. Darrieus in 1927 [1]. A patent of this type of wind turbine was permitted in 1931. However the technology was ignored at that time. Nevertheless, during late 20th century, the National Aerodynamics Laboratory of Canada and Sandia laboratory of the United States have performed a large quantity of experiments about such turbine. It appeared that the power efficiency of the Darrieus type wind turbine rated the highest, compared with other types. The most popular and widely used type of the Darrieus type wind turbine is the H-type. There are certain advantages of the Darrieus type wind turbine, mainly: Omni directionality without a yaw control; better aesthetics to integrate into buildings; more efficient in turbulent environments; and quieter in operation. Nevertheless, a number of constraints such as low starting

torque, high torque fluctuations and complex flow are holding back the potential market of the Darrieus type wind turbine [2].

Given the shortcomings discussed above, a method to figure out how every factors of a wind turbine affecting the power efficiency is urgent to be discovered. This method could be developed into an appropriate typical progress to design a VAWT. Six parameters are ought to be concerned here: installation angle; blade airfoil; chord length; number of blades; radius of an impellor; and wind speed. One part of CFD simulation is set up for each parameter [3].

As a starting point, the series of NACA00 blade airfoil, the most popular shape utilized in both horizontal and vertical axis wind turbine, is introduced to be the test model of the whole simulation process herein.

Based on a great deal of research [4,5,6], although it is less accurate to perform a 2D computation in predicting airfoil stall than a 3D one, the simulation of the whole model in normal condition is still fitted with the actual situation. Wind tip vortex is not taken into account in a 2D simulation, which leads to a little higher power output compared to real condition. In addition, the time consumed in a 2D computation has proved to be far less than in a 3D simulation. So it does have practical significance, therefore in this paper the simulation is conducted in 2D method. Eventually, a series of experiments would be conducted, adopting a spin-up method, and in the process measuring the performance of the wind turbines. Rotating speed of the impellor would be controlled in every step by connecting resistors with different resisting value between the two electrodes of the electric generator. Because the power consumed by resistors equals to the one generated by impellor, torque of the impellor would not need to be measured, which brought in convenience to the experiment.

THE WIND TURBINE MODELING AND CFD SET-UP

The modeling discussed in the present section is a primary one. For each part of simulation, certain modification would be made according to the parameter to be examined in the next section.

The wind tunnel domain

Figure 1 shows the main dimensions and the boundary conditions employed in the wind tunnel domain, representing the outside fluid

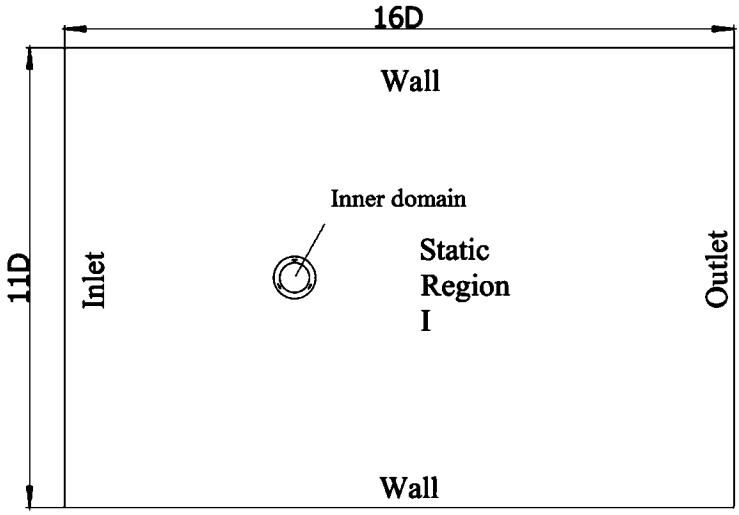

Figure 1. The tunnel domain

around the wind turbine impellor. The outer computational region is suggested to be wide enough so that the effect of the wall is counteracted as much as possible. Here the wind tunnel width was set to 11 times of the diameter of the inner domain. Likewise, the distance not far enough from the inlet of the wind tunnel domain to the inner domain has been proved to give incorrect results of the computation. In order to observe wake formations during the operation of the wind turbine, a far distance from the outlet to the inner domain was set. Due to the complexity of the airfoil, unstructured mesh is more appropriate to adapt to the boundary of the blade. The mesh of the wind tunnel domain is shown in Figure 2.

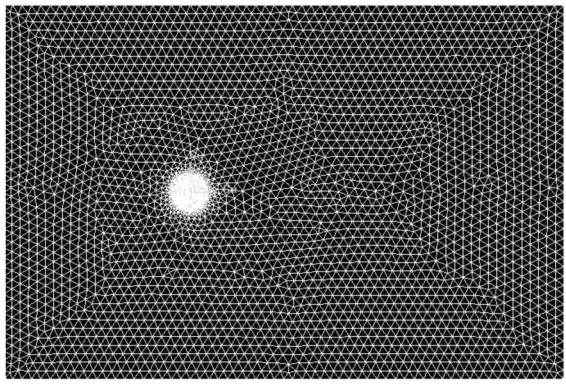

Figure 2. The tunnel domain mesh

The inner domain and meshing

A blade airfoil was exported from a program called NACA airfoil section, which contains all series of NACA

airfoil data. There were three blades in the primary turbine model. As the central column and blade support arms bring minor influence in the simulation, they could be ignored and not showed up in the modeling. The inner domain consists of two regions: Static Region II and Dynamic Region. As shown in Figure 3, Static Region II is a circular subdomain fitted into a ring Dynamic Region which is assumed to be diameter D. Considering the Dynamic Region is the area where blade airfoil is located in, the meshing size was refined independently, as shown in Figure 4. Final meshing work was completed in professional mesh tool GAMIT.

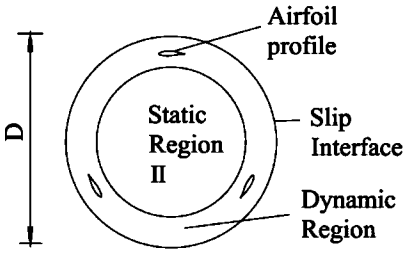

Figure 3. The inner domain

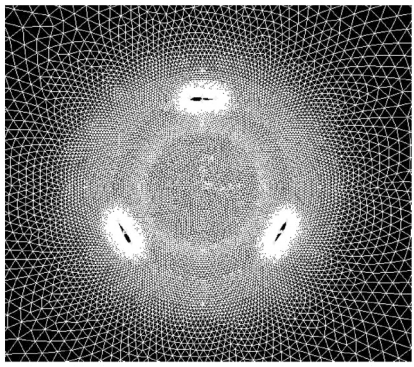

Figure 4. The inner domain mesh

Boundary Conditions

The completed mesh work would be imported into ANSYS Fluent, which was applied to accomplish CFD simulation task [7]. After that, boundary condition was bound to be set. The Inlet was set to a speed of 10m/s, oriented right. The Outlet was set to pressure outlet, relatively 0Pa. Meanwhile, for Dynamic Region, an anticlockwise angular velocity ω was imposed to simulate rotating motion of the wind turbine impellor. Walls were defined to both sides of the wind tunnel, meaning no slide at this boundary. A slid interface boundary was employed between the Static Region I and the Dynamic Region in order to guarantee fluid continuity and faster result convergence. The same principle was applied between Dynamic Region and Static Region II in the inner domain.

The transient solver settings and turbulence model

Transient calculations are related to time. The steps of calculation and time of single-step are required to set in Fluent. The shorter of the computing time of single-step, the more accurate the result is, but it

takes more time. Taking into account of the actual situation, the wind turbine was set to rotate 2° in every single step. The rotary motion of the computational domain was defined by a given speed. Due to the different stream velocity, the actual speed range of the wind turbine is different. The time that two degrees of rotation of the wind turbine takes can be calculated by the given speed of wind turbine:

$$t = \frac{2\pi}{180\omega} = \frac{\pi}{90\omega} \tag{1}$$

In advance an initial value is given, and then gradually equation iterated. Finally the exact figure would be obtained approximately. In present example, the wind turbine rotation was set for two turns, and then the total number of iterations would be 720 steps, which means that in each step of time, the iteration step of calculation was 180 steps. RNG turbulence model was employed for the actual calculation. Based on the pressure implicit Spalart-Allmaras algorithm, the second-order upwind difference scheme was chosen. The global iterating error of each variable's value has been proved to be less than 10^{-7}, which is considered to meet the accuracy requirements.

RESULTS

In this section, each of six parameters is evaluated through CFD simulation. For each case, the variables monitored were the power coefficient C_p versus Tip Speed Ratio (TSR). The power coefficient C_p is given by [8]:

$$C_p = \frac{P_I}{0.5\rho A_r U_\infty^3} \tag{2}$$

And the TSR as:

$$TSR = \frac{\omega R_r}{U_\infty} \tag{3}$$

Table 1 summarizes all modelling parameters, including those defined and used in the two equations above and those to be utilized next, in simulating the following six (6) cases, one for each design parameter, with their respective symbols and units.

Table 1. List of parameters presented in the equations.

Parameter	Symbol	Unit
Power coefficient	C_p	
Tip speed ratio	TSR	
Constant wind speed	U_∞	[m/s]
Angular velocity	ω	[rad/s]
Rotor radius	R_r(r)	[m]
Power of impellor	P_I	[W]
Power of wind	P_W	[W]
Torque of impellor	T_I	[Nm]
Air density	ρ	[kg/m^3]
Rotor swept area	A_r	[m^2]
Voltage output	U	[V]
Resisting value	R	[Ω]
Rotating speed	n_I	[r/min]
Number of blades	N	
Chord length	c	[mm]
Solidity of impellor	σ	

Case 1: Installation Angle

In case 1, a NACA0018 was chosen as an airfoil. The aim was to verify how the power efficiency changes in different installation angle. The initial design data of the blades is listed in Table 2. Figure 5 shows how an installation angle is defined. It is an angle between chord line and

tangential direction. A constant wind speed U_α of 10m/s was chosen with the impeller operating at 8 different TSR values, for a series of installation angle at 0°, 4°, 5°, 6°, and 8°.

As shown in Figure 6, each curve represents a C_p tendency versus 8 different TSRs. As can be seen, the highest C_p for 5° curve is achieved at TSR of 2.0, while no obvious diversity for each installation angle situation could be peeked. This means that the wind turbine achieves peak power efficiency with a blade installation degree of 5, reaching 41.57%.

Table 2. Initial design data of the blades

N(number of blades)	c(mm)	R_T(mm)
3	140	500

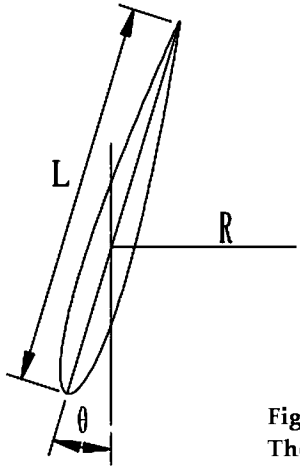

Figure 5.
The installation angle

Case 2: Blade Airfoil

In response to the outcome from Case 1, an installation angle of 5° was determined. In Case 2, the chord length would remain 140mm, with number of blades 3 and constant wind speed of 10m/s. In this case, a series of NACA airfoil were examined, including 0012, 0015, 0018, and 0020. The aim was to verify how the power generated was affected by different airfoil versus different TSRs. For each airfoil, 8 different TSRs were considered in order to show the performance of the impeller when operating both at optimum and lower values.

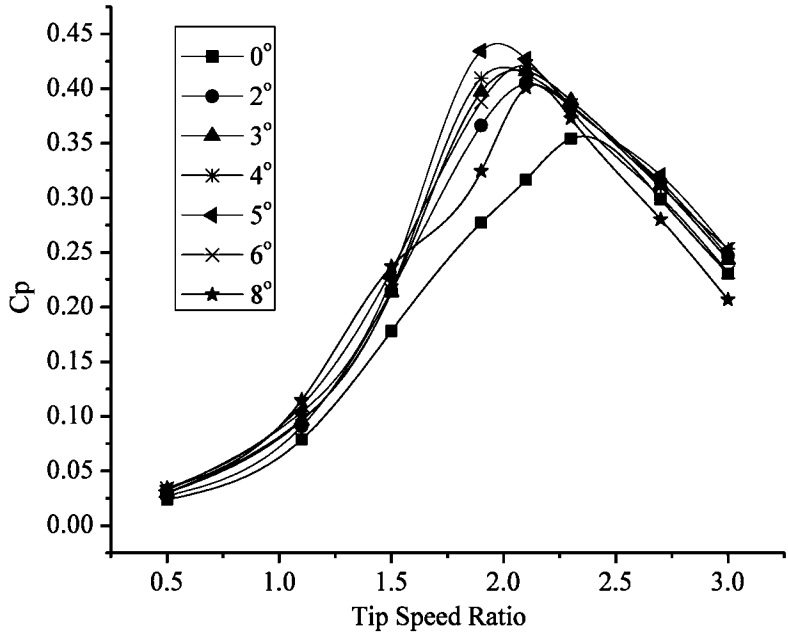

Figure 6. Power coefficient C_p versus TSR for different installation angle

Figure 7 shows the C_p as a function of TSR for different airfoil. As can be seen that for 0015, C_p exceeds others slightly for TSR values lower than the maximum, while it is almost invariant on the right side. It means that 0015 is relatively more adaptable for low TSR.

Case 3: Chord Length

In this case, the chord length would be a variable to be considered. The chord length represents the size proportion of the blade, when the other design parameter is unvaried. The aim of this case was to determine which chord length was more appropriate in given installation angle, number of blades, and constant wind speed of 10m/s. The to be examined chord length would include 100mm, 130mm, 140mm, 150mm, 180mm. For each one, 8 different TSRs were considered.

Figure 8 shows the C_p as a function of TSR for different chord length. It can be seen, in a low TSR, the C_p increases slightly with chord length increasing before reaching the maximum values. This trend means increasing the chord length could improve self-starting performance. It also can be seen that for the chord length of 130mm, the C_p

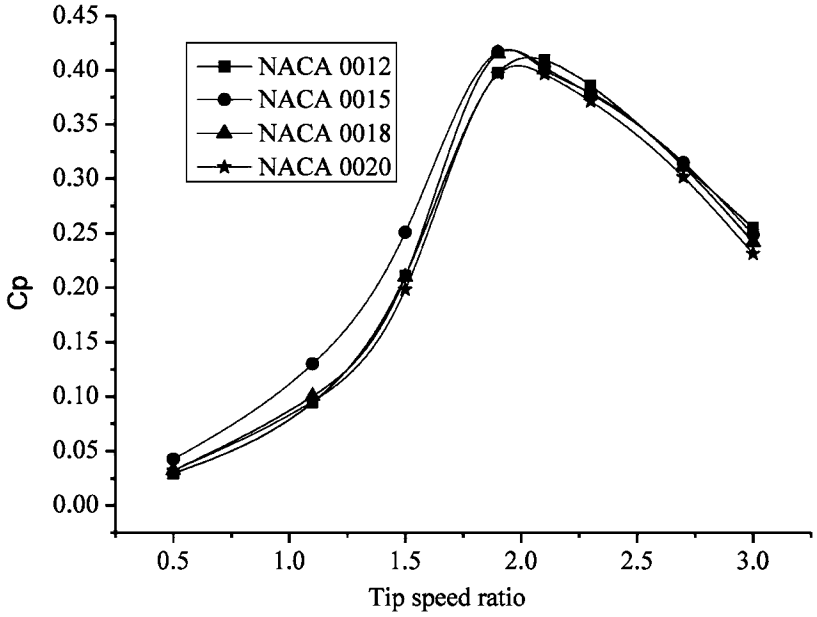

Figure 7. Power coefficient C_p versus TSR for different blade airfoil

increases with the TSR, with a peak value of 0.4402 at TSR of 2.3, while for 140mm chord length with a peak value of 0.4343 at TSR of 1.9. The diversity of peak value is minor, while a chord length of 140mm self-starting performance, which would be selected as the relatively ideal chord length.

Case 4: Number of Blades

Hereto, what have been pinned down include installation angle (5°), blade airfoil (NACA 0015), and chord length (140mm). How number of blades affecting performance of a wind turbine would be figured out in present case. With the constant wind speed remaining 10m/s, four blades number were examined, including 2, 3, 4, and 5. For each number of blades, 8 different TSRs were considered in order to show the performance of the impellor when operating both at optimum and lower values.

Figure 9 shows the C_p as a function of TSR at four different number of blades. It is clearly shown that the diversity of C_p is much more obvious at higher TSR then at lower one. For a 2 blades impellor, the C_p in-

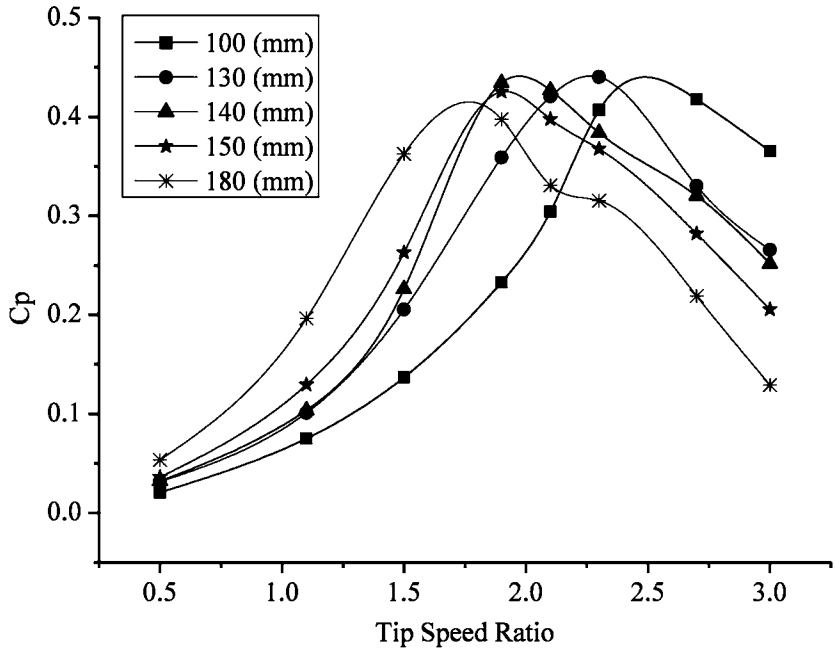

Figure 8. Power coefficient C_p versus TSR for different chord length

creases with the TSR, with a peak value of 0.4498 at TSR of 2.3. However, at low TSR scenario, the power efficiency of a 2 blades impellor is so low that it should be dismissed. Comparing with a 2 blades impellor, a 3 blades one reaches a peak value of 0.4343 as TSR is only 1.9. Therefore, 3 blades were confirmed.

Case 5: Radius of an Impellor

In response to the tendency that the vertical axis wind turbines worldwide have been designed bigger and bigger, how a wind turbine's behavior is affected due to different radius of impellor was to be examined. In previous cases, these parameters have been presented: installation angle, blade airfoil, chord length, and number of blades. The constant wind speed would remain 10m/s. The to be examined radius of impellor varied from 300mm to 700mm, totally 5 different radiuses.

Figure 10 shows the C_p as a function of TSR for different radius value. It appears that for varied radius, the C_p follows an entirely opposite tendency between low TSR and high TSR. At low TSR, the shorter

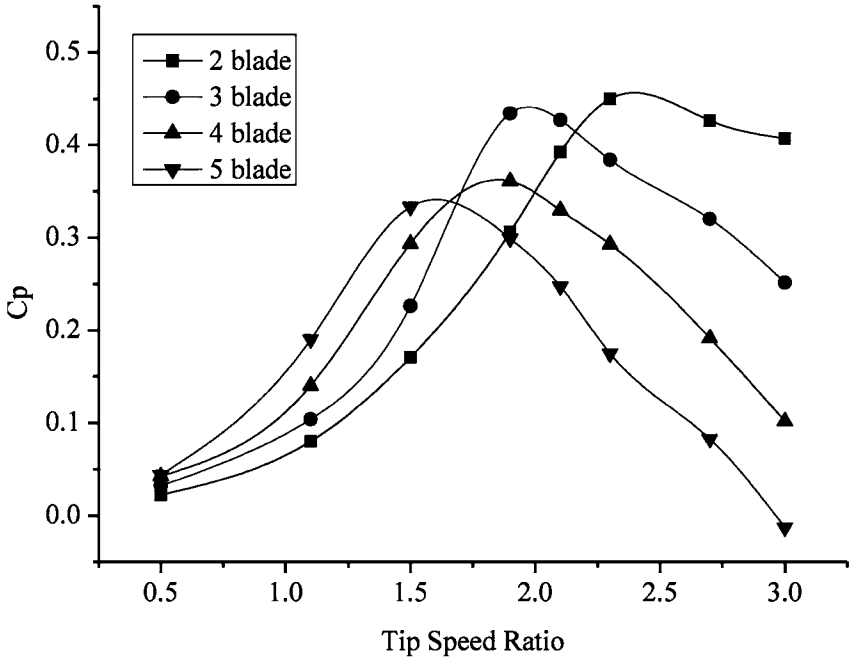

Figure 9. Power coefficient C_p versus TSR for different number of blades

the radius is, the higher the C_p gains. It means that a VAWT with a narrower impellor would take less effort to self-start. At high TSR, the longer the radius is, the higher the C_p gains, meaning that a VAWT with a wider impellor would reach higher power efficiency in high speed operating stage.

Figure 11 shows the power as a function of TSR for different radius value. It can be seen that the power output increases dramatically for TSR values higher than the maximum as the radius got longer, while it is almost invariant on the left side. So it comes down to a dilemma how to select an appropriate radius of an impellor. It is dependent on the space where the wind turbine is constructed, and the cost to build a turbine. In this article, a compromising method is adopted, a radius of 500mm being chosen.

So far, the parameters to design a vertical axis wind turbine have all been examined through CFD simulation. The determined values are listed in Table 3.

Table 3. The determined values of designing a VAWT

Installation angle	Blade airfoil	Chord length (mm)	Number of blades	Radius of impellor (mm)
5°	NACA0015	140	3	500

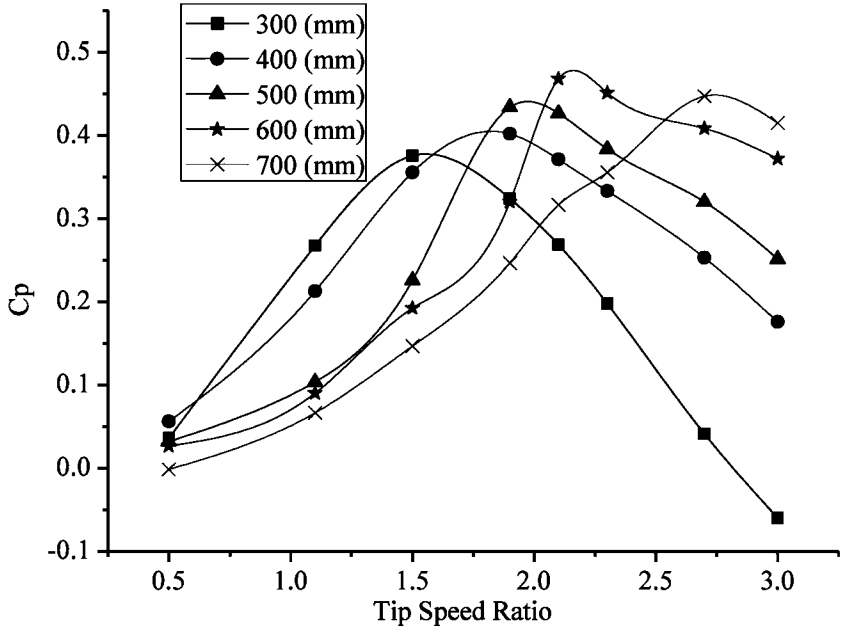

Figure 10. Power coefficient C_p versus TSR for different radius of impellor

Case 6: Wind Speed

Through previous cases, a basic wind turbine has been fully designed. In case 6, the wind speed would be a variable, ranging from 2m/s to 15m/s. For each wind speed U_α 8 different TSRs were considered to show the performance of the impellor when operating both at optimum and lower values. Both the power coefficient C_p and power output were monitored during the computation.

Figure 12 shows the C_p as a function of TSR for different wind speeds. The overall C_p follows the same trend independently of the wind speed considered. It implies that C_p is a characteristic parameter of the wind turbine and it would not diver as wind speed changes.

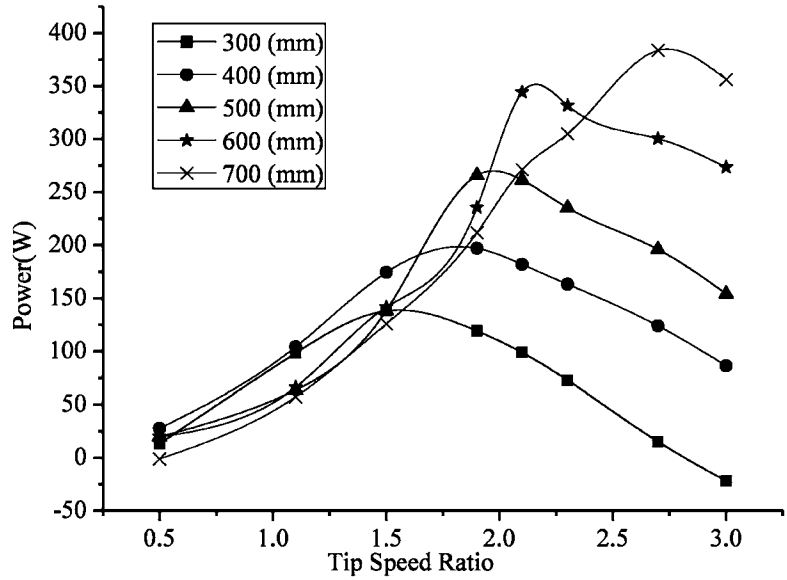

Figure 11. Power output versus TSR for different radius of impellor

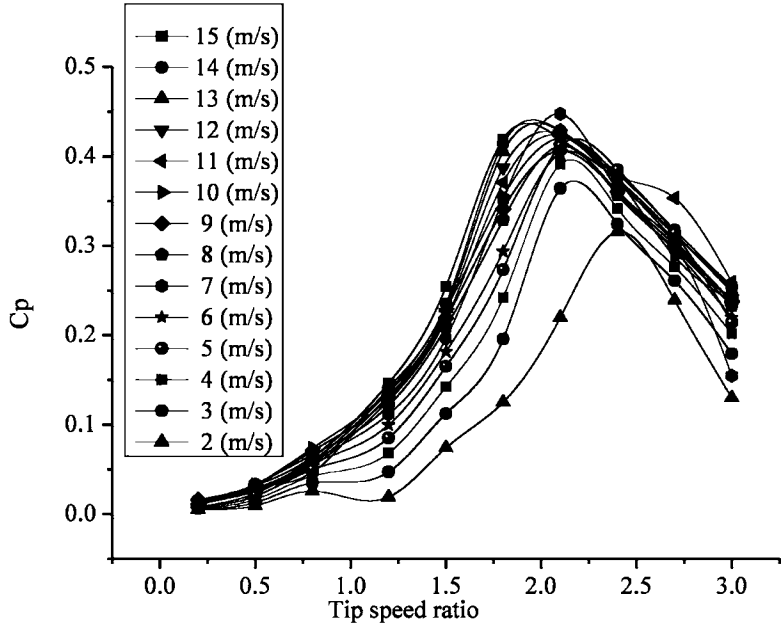

Figure 12. Power coefficient C_p versus TSR for different wind speed

Figure 13 shows the power output as a function of TSR for the same range of wind speeds. It can be seen that the power output increases with the TSR, with a peak value at TSR of approximately 2.0, and then decreases linearly afterwards. It also can be seen that when TSR is unvaried, the power output increases as wind speed picks up.

DISCUSSION ON THE SIMULATION RESULTS

In the previous section, 6 cases were proposed to evaluate the performance of a straight-bladed VAWT. The first 5 cases are related to characteristic parameters that are essential to design a VAWT. The respective C_p were evaluated and presented in a diagram. How every parameter affects the performance of impellor was analyzed one after another in a certain order. This order is supposed to be developed into a standard design flow of a VAWT. In case 1 and 2, where the installation angle and blade airfoil were examined, the different effect couldn't distinctively

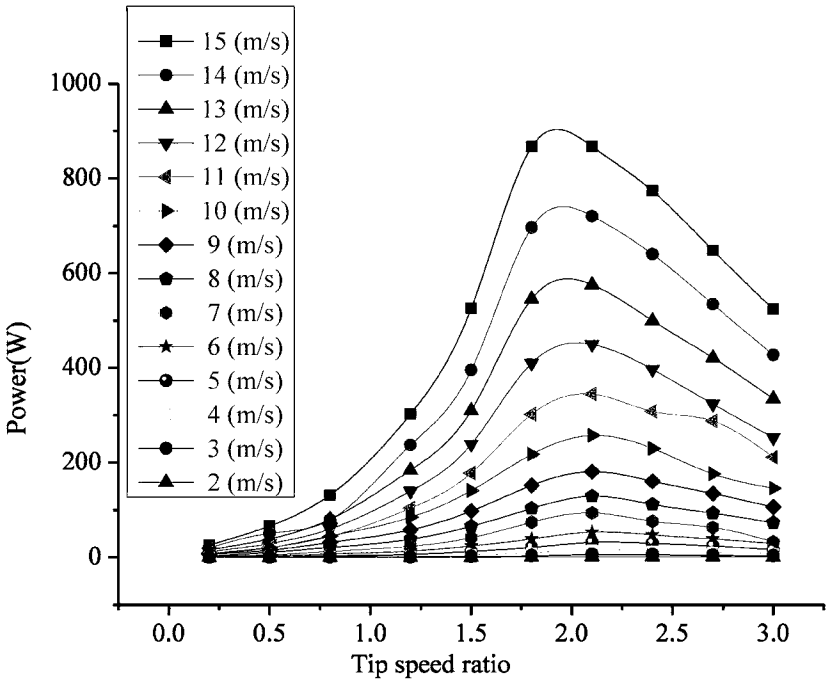

Figure 13. Power output versus TSR for different wind speed

tell, so a relatively higher value was chosen. In case 3, several peak values were not shown up at the same TSR, so a moderate value was chosen. In case 4, after comparing the performance comprehensively, proper number of blades was determined. In case 5, it appeared that for varied radius, the C_p followed an entirely opposite tendency between low TSR and high TSR. The higher C_p at both lower and higher TSR were not adopted. A compromising value of radius of impellor was selected.

The 6th case has been proved to not be the characteristic parameter of a VAWT. It was actually the operating condition exerted by external environment. It has shown, not surprisingly, that as wind speed picks up, the power generated increases.

EXPERIMENTAL SET-UP

Experiment facilities

In this experiment, an air blower is used to generate wind which drives the wind turbine to spin. The reason why we do not apply a wind tunnel is that an air blower might exactly generate wind that contains turbulence, more similar to the wind of the nature. The uncertainty and randomness of the nature wind have to be simulated in this experiment. The air blower used here is an axil wind blower SFNO7-4, generating wind of 10m/s average.

The wind speed is recorded by a digital air flow anemometer GM816/8908, ranging 0 to 30m/s of wind speed, with an error ±5%.

The electric generator is mounted below the impellor of the wind turbine, connected with a pair of gear. The electric generator is a type of TX3420D120, with a rated rotating speed of 3000 r/min, output voltage of 150V.

The rotating speed of the turbine is recorded by a photoelectric tachometer Fluke 931. A tape reflecting light is pasted at the side of the rotating spindle.

Experimentation Method

Measurement of the steady impellor power was carried out using an indirect method following a spin up procedure, opposite to one developed by Edwards et al [9]. The spin up procedure is due to the consideration that the starting up performance of the turbine would be revealed when the turbine picks up rotating speed from the static state.

A series of resistor was connected between both electrodes of the electric generator, so as do a voltmeter. In order to portray the C_p curve, different resistors would be applied to this circuit, starting with low resisting value then higher one. For each resistor, when the turbine spinning was steady, the consuming power of the resistors would be equal to the output power of the electric generator, also to the wind absorbing power of the impellor, as shown in Eqs. (4) (5) and (6).

$$C_p = \frac{P_I}{P_w} = \frac{T_I \omega}{\frac{1}{2}\rho A_r V_\infty^3} \tag{4}$$

$$T_I \omega = \frac{U^2}{R} \tag{5}$$

$$\omega = \frac{2\pi n_I}{60} \tag{6}$$

In this way, two quantities would be measured directly, U_α and N_I, which are convenient to measure, avoiding measuring the torque of the impellor. The steady wind generated by wind blower has been measured in ahead, which is 10m/s in average. And the resistors connected have known resisting value, as shown is Figure 14. The measurement of the TSR is shown as Eq. (3).

Wind Turbine Model

As can be seen in the CFD simulation part, three parameters evidently distinguished the performance of the wind turbine, number of blades, and radius of impellor and chord length. Therefore, the tested model of the turbine, as shown in Figure 15, took in the consideration of these there parameters. Each of the parameters is labeled as Table 4. Each parameter combines with each other in order as shown in Table 5, considering the convenience and effectiveness of assembling and disassembling.

EXPERIMENTAL RESULTS

After each of the model turbines were tested, the results revealed that they could be divided into three groups according to the performance.

Table 4. The distinguish of the three parameters for each value

Number of blades			Radius of impellor (mm)		Chord length (mm)		
A_1=2	A_2=3	A_3=4	B_1=300	B_2=250	C_1=100	C_2=150	C_3=160

Table 5. The combination of each parameter

Combinations with B_2	Combinations with B_1
$A_3B_2C_2$	$A_2B_1C_3$
$A_1B_2C_2$	$A_2B_1C_2$
$A_1B_2C_1$	$A_2B_1C_1$
$A_3B_2C_1$	$A_1B_1C_3$
$A_3B_2C_3$	$A_1B_1C_2$
$A_1B_2C_3$	$A_1B_1C_1$
$A_2B_2C_3$	
$A_2B_2C_2$	
$A_2B_2C_1$	

Idle Group

Models sorted in idle group means the model of the turbine could barely rotate under the same given wind speed. Examining these turbines, one thing is obvious. They are both with less number of blades and with short chord length. Solidity would be used to explain why this pattern occurs. Solidity is given by Eq. (7).

Figure 14. Resistor module with known resisting value

Figure 15. Tested model of the VAWT

$$\sigma = \frac{Nc}{r} \tag{7}$$

Experiment considering solidity has been conducted Okeoghene et al. [10]. revealing that the shift of the entire CP-TSR curve of the higher solidity VAWT to the left, hence attaining maximum CP at lo wer TSR,

Table 6. Model turbines grouped according to the performance

Idle Group	Low-effective Group	High-effective Group
$A_1B_2C_1$	$A_1B_2C_3$	$A_3B_2C_2$
$A_2B_2C_1$	$A_1B_2C_2$	$A_2B_1C_3$
$A_1B_1C_2$	$A_2B_2C_2$	$A_2B_1C_2$
$A_1B_1C_1$	$A_3B_2C_1$	$A_1B_1C_3$
$A_2B_1C_1$	$A_2B_2C_3$	

while the lower solidity VAWT attained maximum CP at higher TSR, the same trend as shown in Figure 8, 9, and 10. This suggests that when a VAWT is to be designed, it might have to be prudent to choose one with both less number of blades and short chord length.

Low-effective Group

All the turbine models that were classified into low-effective group revealed a pattern that they were with respectively shorter radius of impellor. It could be explained that with the same force coming from blades, an impellor with shorter support arms would form lower driving torque, which confronts the resisting torque formed by the loads.

As can be seen in Figure 16 and Figure 17, increasing the number of blades contributes to improve the voltage output and CP of a turbine, otherwise the chord length must keep up to a certain level in order to compensate the loss of power. It also can be seen that both the CP and TSR in Figure 17 are far too low, due to the producing and assembling error of the turbine. Additionally, the turbine prototype is in testing size. According to Eqs. 2 and 3, when the size of the model is small, the TSR would be low, and that decides the low CP.

High-effective Group

The effect of the radius of impellor in high-effective group is the same to the one mentioned in low-effective group: higher performance with longer supporting arms. Furthermore, the contribution of the number of blades and chord length follows the same regularity.

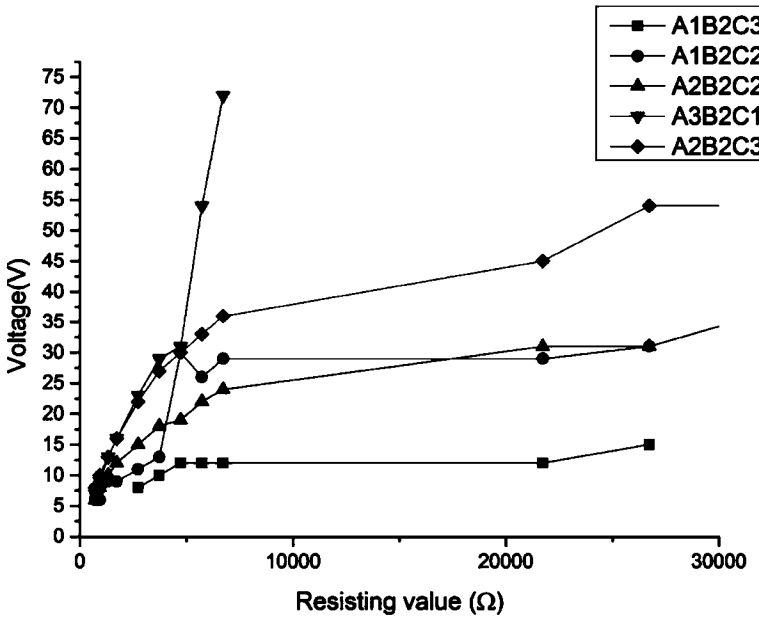

Figure 16. Voltage output versus resisting value for different VAWT models

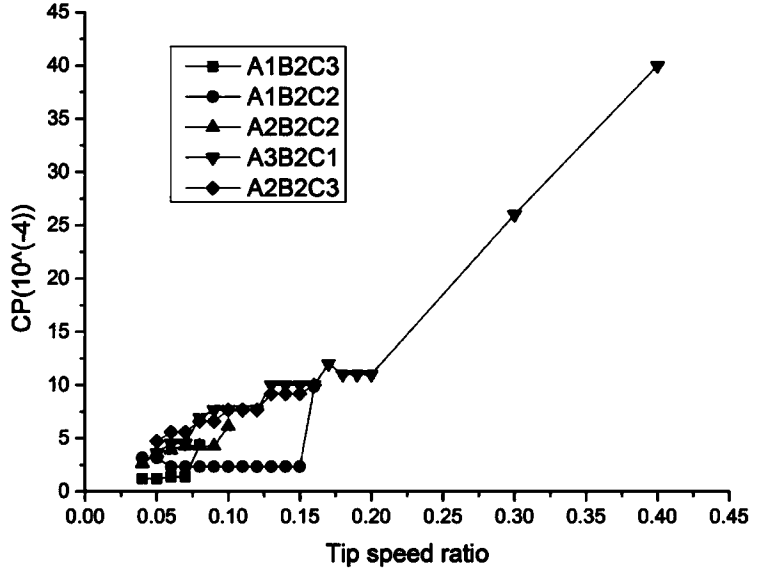

Figure 17. CP versus TSR for different VAWT models

Nonetheless, some unexpected phenomenon occurs in the high-effective group. Several turbine models got abrupt increase before reaching peak power output point, like A3B2C2 and A1B1C3. The peak has been lagged respectively. Considering the solidity, these two turbines belong to lower solidities. Although it reveals that these types of turbine would be more difficult to start rotating at the beginning, their peak points went far higher than the other ones eventually, as can be seen in Figure 18 and 19. When a turbine is to be put into low wind environment, then it requires self-starting ability, which means higher solidity. Otherwise, a turbine can be designed to low solidity in order to gain more power when it is fully revolving.

CONCLUSIONS

By CFD simulation, the parameters affecting performance of a VAWT have been scrutinized one by one, and three of them, number of blades, radius of impellor and chord length, were referred to be essential for a VAWT. These three parameters have constituted the solidity. Having conducted the experiment in the same wind speed of 10m/s, models

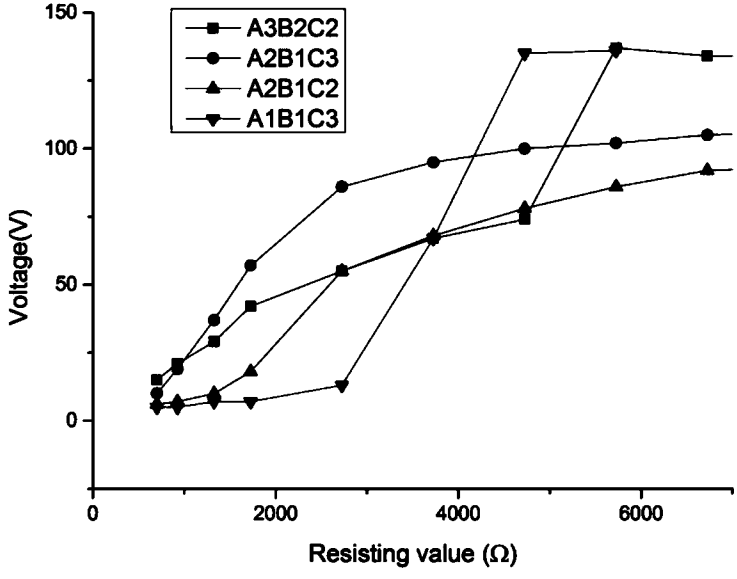

Figure 18. Voltage output versus resisting value for different VAWT models

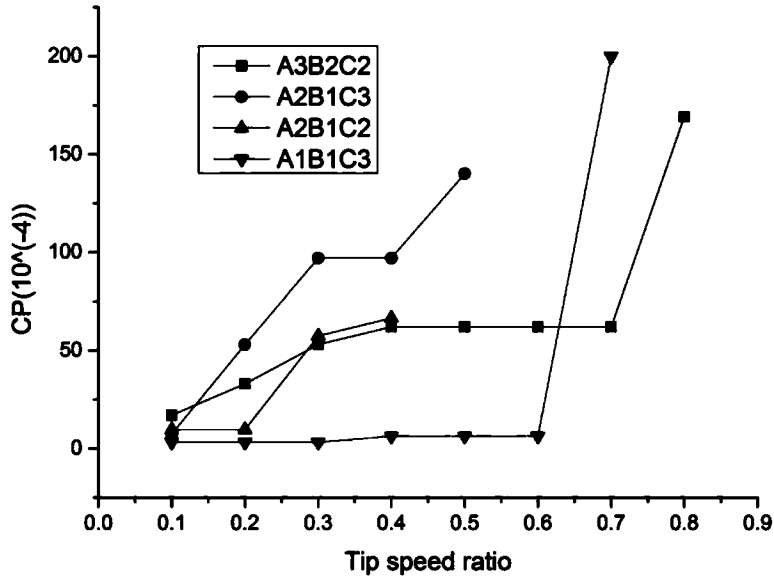

Figure 19. CP versus TSR for different VAWT models

of the turbine have been grouped according to the performance. The idle group reveals that less number of blades and short chord length would be a fatal combination of factors for a turbine. The low-effective group suggests that a turbine might have a properly long supporting arm. The high-effective group concludes that low solidity for high wind environment and high solidity for low wind environment, considering the self-starting ability.

Future work

Due to the limit of conditions of experiment, the turbine models having been tested were in prototype. The TSR and CP were not complete. Next work would be constructing larger turbine. The constructing and assembling accuracy also should be improved.

Acknowledgements

This work was completed under the supports of National Natural Science Foundation of China (51376096) and Workstation of business graduate student of Jiangsu province.

References

1. Sandra Eriksson, Hans Bernhoff, Mats Leijon. Evaluation of Different Turbine Concepts for Wind Power [J]. *Renewable and Sustainable Energy Reviews*, 2008, 12: 1419- 1434
2. Rosario Nobile, Maria Vahdati, Janet F. Barlow, et al. Unsteady Flow Simulation of a Vertical Axis Augmented Wind Turbine: A Two-Dimensional Study [J]. *Journal of Wind Engineering and Industrial Aerodynamics*, 2014, 125: 168-179
3. Qiaomei Li. Aerodynamic Performance Analysis and Airfoil Optimization on Miniwatt Vertical Axis Wind Turbine [D]. Nantong: Nantong University, 2014
4. Jian Li, Xianju Meng, Shaofeng Li, Rongjian Zhang. Installation Angle CFD Analysis of a Small H-type VAWT [J]. *Journal of Hebei Polytechnic University* (Natural Science Edition), 2011, 33(4)
5. Faming Wu. Research on Straight-Bladed Vertical Axis Wind Turbine [D]. Lanzhou: Lanzhou University of Technology, 2009
6. S. Rolland, W. Newton, A.J. Williams, T.N. Croft, D.T. Gethin, M. Cross, Simulations Technique for the Design of a Vertical Axis Wind Turbine Device with Experimental Validation [J]. *Applied Energy*, 2013, 111: 1195-1203
7. Shuxue Liao, Chun Li, Jiabin Nie, Wei Guo. The Analysis of Aerodynamic Performance for Small H-type VAWT Based on Different Airfoils [J]. Machine Design and Research, 2011, 27(3)
8. Mojtaba Ahmadi-Baloutaki, Rupp Carriveau, David S.-K. Ting. Performance of a Vertical Axis Wind Turbine in Grid Generated Turbulence [J]. Sustainable Energy Technologies and Assessments, 2015
9. Edwards JM, Danao LA, Howell RJ. Novel experimental power curve determination and computational methods for the performance analysis of vertical axis wind turbines [J]. *Sol Energy Eng* 2012; 134(3):11.
10. Okeoghene Eboibia, Louis Angelo M. Danao, Robert J. Howell Experimental investigation of the influence of solidity on the performance and flow field aerodynamics of vertical axis wind turbines at low Reynolds numbers [J]. *Renewable Energy* 2016

ABOUT THE AUTHORS

Yang Cao, School of Mechanical Engineering, Nantong University, Nantong 226019, P.R. of China; Jiangsu Engineering Research Center of Wind Energy Application, Nantong 226019, P.R. of China.

Jinyi Li, School of Mechanical Engineering, Nantong University, Nantong 226019, P.R. of China; School of Mechanical Engineering, Nantong University, Nantong 226019, P.R. of China.

Guoqing Wu, School of Mechanical Engineering, Nantong University, Nantong 226019, P.R. of China; Jiangsu Engineering Research Center of Wind Energy Application, Nantong 226019, P.R. of China.

Qiaomei Li, School of Mechanical Engineering, Nantong University, Nantong 226019, P.R. of China.

Yujuan Shi, School of Mechanical Engineering, Nantong University, Nantong 226019, P.R. of China.

Shuda Xing, School of Mechanical Engineering, Nantong University, Nantong 226019, P.R. of China.